IEEE Access
Multidisciplinary | Rapid Review | Open Access Journal

Received 3 March 2023, accepted 11 March 2023, date of publication 16 March 2023, date of current version 22 March 2023.

Digital Object Identifier 10.1109/ACCESS.2023.3257988

RESEARCH ARTICLE

Internet of Things and Deep Learning Enabled Diabetic Retinopathy Diagnosis Using Retinal Fundus Images

THANGAM PALANISWAMY, (Member, IEEE), AND MAHENDIRAN VELLINGIRI
Department of Electrical and Computer Engineering, Faculty of Engineering, King Abdulaziz University, Jeddah 21589, Saudi Arabia

Corresponding author: Thangam Palaniswamy (tswamy@kau.edu.sa)

The authors extend their appreciation to "the Deputyship for Research & Innovation, Ministry of Education in Saudi Arabia for funding this research work through the project number G: 693-144-1443" and King Abdulaziz University, Deanship of Scientific Research (DSR), Jeddah, Saudi Arabia.

ABSTRACT Recently, the Internet of Things (IoT) and computer vision technologies find useful in different applications, especially in healthcare. IoT driven healthcare solutions provide intelligent solutions for enabling substantial reduction of expenses and improvisation of healthcare service quality. At the same time, Diabetic Retinopathy (DR) can be described as permanent blindness and eyesight damage because of the diabetic condition in humans. Accurate and early detection of DR could decrease the loss of damage. Computer-Aided Diagnoses (CAD) model based on retinal fundus image is a powerful tool to help experts diagnose DR. Some traditional Machine Learning (ML) based DR diagnoses model has currently existed in this study. The recent developments of Deep Learning (DL) and its considerable achievement over conventional ML algorithms for different applications make it easier to design effectual DR diagnosis model. With this motivation, this paper presents a novel IoT and DL enabled diabetic retinopathy diagnosis model (IoTDL-DRD) using retinal fundus images. The presented Internet of Things Deep Learning – Diabetic Retinopathy Diagnosis (IoTDL-DRD) technique utilizes IoT devices for data collection purposes and then transfers them to the cloud server to process them. Followed by, the retinal fundus images are preprocessed to remove noise and improve contrast level. Next, mayfly optimization based region growing (MFORG) based segmentation technique is utilized to detect lesion regions in the fundus image. Moreover, densely connected network (DenseNet) based feature extractor and Long Short Term Memory (LSTM) based classifier is used for effective DR diagnosis. Furthermore, the parameter optimization of the LSTM method can be carried out by Honey Bee Optimization (HBO) algorithm. For evaluating the improved DR diagnostic outcomes of the IoTDL-DRD technique, a comprehensive set of simulations were carried out. A wide ranging comparison study reported the superior performance of the proposed method.

INDEX TERMS Computer aided diagnosis, deep learning, diabetic retinopathy, fundus images, honey bee optimization.

I. INTRODUCTION

IoT is defined as practice of molding and designing Internet-connected Things by computer networks. The word'Io' indicates instead of utilizing smaller effective devices such as smart phone, laptops, and tablets, it can be better to utilize a number of minimal effectual gadgets like fridges, wrist bands, umbrellas, Air Conditioners (AC), etc. [1]. IoT method will support cloud computing (CC) for enhancing the operation regarding higher resource application, memory, power along with computational capability. Moreover, CC obtains advantages from IoT via rising its scope for managing real-time applications and providing many services in dynamic format and distributed way [2]. The IoT-related CC is expanded for advancing innovative services and applications in a healthcare platform. In the year 2017, nearly 451 million individuals

The associate editor coordinating the review of this manuscript and approving it for publication was Carmelo Militello.

suffered from this disease [3]. A high blood sugar level severely weakens body organs and causes complications like retinopathy, coronary episode, cataracts, vision loss, dementia, and glaucoma. A rising population, irrespective of age, suffering from diabetic mellitus has issues in vision called DR [4]. Though DR is mostly symptomless in the initial levels, neural retinal damage and clinically unseen micro vascular changes grow at the time of initial phases. Therefore, regular eye screening is mandated for patients affected by diabetes, as prompt diagnosis of the condition becomes necessary [5]. Though earlier identification of DR depends upon operational changes in Electro Retino-Graphy (ERG), retinal blood vessel caliber, and retinal blood flow, in medical practices initial identification depends on fundus analysis [6]. Fundus photography was a well-tolerated, rapid, non-invasive, and broadly accessible that forms one method that is mostly utilized for assessing the extent of DR [7]. Using fundus images, ophthalmologists monitor retina lesions at higher resolution for diagnosing DR and predicting its severity. But manually DR identification from fundus images requires higher level of expertise and effort by a specialized ophthalmologist, particularly in remote areas or densely populated counties such as Africa and India [8], wherein the number of people with DR and diabetes can be projected to increase dramatically in the following years, whereas the ophthalmologists are disproportionally low. This has induced the research field for advancing computer-aided diagnosis (CAD) system that minimizes the effort, cost, and time required by a medical professional for identifying DR [9]. New progressions in Artificial Intelligence (AI) and the rise of computation resources and abilities have constituted the opportunity for advancing deep learning applications for precise DR classification and detection [10].

This paper presents a novel IoT and DL enabled diabetic retinopathy diagnosis model (IoTDL-DRD) using retinal fundus images. The presented IoTDL-DRD technique utilizes IoT devices for data collection purposes and then transfers them to the cloud server to process them. Followed by, the retinal fundus images are preprocessed to remove noise and improve contrast level. Next, mayfly optimization based region growing (MFORG) based segmentation technique is utilized to detect lesion regions in the fundus image. Moreover, densely connected network (DenseNet) based feature extractor and long short term memory (LSTM) based classifier is used for the effective DR diagnosis. Furthermore, the parameter optimization of the LSTM model is carried out by honey bee optimization (HBO) algorithm. For evaluating the improved DR diagnostic outcomes of the IoTDL-DRD technique, a comprehensive set of simulations were carried out.

II. LITERATURE REVIEW

Rajavel et al. [11] present a stochastic neighbor embedding (SNE) feature extracting technique with a view to removing unnecessary noise and dimensional reduction from the fundus images. Once the extraction of features is done, the presented optimized deep belief network (O-DBN) classification method can measure the image features into different classes that provide the severity level of DR disease. The researchers in [12] devise a DL-enabled optimized feature selection technique for classifying the phase of DR severity from the fundus image. The candidate lesion regions are identified with the help of an Attention-based Fusion Network (AFU-Net). Afterward, texture and shape features were derived, and consequently, optimum feature subset was chosen by making use of the Improved Harris Hawk Optimizing technique. At last, a deep CNN categorizes the DR phases, and the model weight can be updated through the same technique.

In [13], modelled an Autoregressive-Henry Gas Sailfish Optimization (Ar-HGSO)-related DL method for identifying DR and severity level classifiers of DR and Macular Edema (ME) related to color fundus images. The segmenting procedure becomes highly essential for correct identification and classifying procedure that segregates the image into several subgroups. The DL technique can be used for effectual detection of DR and severity classification of ME and DR. Further, the DL approach can be well-trained by the proposed Ar-HGSO method to gain superior outcomes. Aljehane [14] presents an intelligent moth flame optimization with Inception network-based DR detection and grading (IMFO-INDR) approach. The aim of this IMFO-INDR algorithm was to identify the presence of lesions from the fundus image and allot suitable class labels to it. Inception v4 method can be implemented as extracting feature and the hyper-parameters indulged in it were done optimal tuning by using MFO approach. Finally, SoftMax classifier can be employed for allocating class labels to the input fundus images.

Gunasekaran et al. [15] use RNN for the purpose of retrieving features from deep networks. So, utilizing computational techniques for identifying some ailments automatically becomes effective solution. The author tested and advanced numerous iterations of a DL structure for forecasting the development of DR in diabetic persons who experienced teleretinal DR assessment. A collection of 3-or 1-field color fundus pictures is the input for both iterations. Using the presented DRNN method, advanced detection of the diabetic state has been carried out by HE identified in a blood vessel of eyes. Gupta et al. [16] project an Optimal Deep CNN for Retinal Fundus Image Classification (ODCNN-RFIC) approach. The proposed method includes preprocessing in 2 stages they are Adaptive Median Filter (AMF) and Guided Filter (GF). The U-Net method was used for segmenting images, permitting the detection of infected regions appropriately. In [17], a new 2-phase Glaucoma Diagnosis Network (ODGNet) and Optic Disk localization were presented. In the initial stage, a visual saliency map merged with shallow CNN can be employed for effective OD localizing from the fundus images. In the second stage, the TL-related pre-trained methods were employed for glaucoma diagnosis.

III. PROPOSED MODEL

In this paper, a novel IoTDL-DRD method was projected for DR detection and classification on retinal fundus images.

The presented IoTDL-DRD method allows the IoT devices for data collection purposes and then transfers to the cloud server to process them. Then, the retinal fundus images are preprocessed for noise removal and contrast improvement. Afterward, the MFORG technique was utilized for lesion segmentation in the fundus images. For DR recognition and classification, the HBO algorithm with LSTM model is exploited. Figure 1 depicts the block diagram of IoTDL-DRD approach.

A. IMAGE PRE-PROCESSING

At the primary level, the IoT devices capture the retinal fundus images and forward them to the cloud server for further examination. Next, the median filtering (MF) technique is used to remove noise and CLAHE is applied to improve contrast level [18]. CLAHE algorithm is extremely effectual in biomedical image analyses and is chiefly utilized for improving the contrast level of an image. This method needs a set of two input parameters such as dimension of clip limit and sub window. In such a way, the presented algorithm recognizes the grid size of window, and also the grid value originated from top left corner area of an image where the computation starts from preliminary index of window. For every grid point, the histogram of region H I1/2 nearby the image is defined. Then, the histogram is presented over the level of estimated clip limit is trimmed and the Cumulative Distributive Function (CDF) is evaluated. The CDF is evaluated for pixel and the value based on 0 to 255. Following, for all the pixels, the four nearby neighboring grid points should be found. By employing the intensity rate, viz, the pixel index, and the mapping functions of the 4 grid points, CDF measure is evaluated. However the procedure is ended, still it accomplishes the concluding index of a window. Computer vision is a subset of the Deep Learning model, enables the computer to possess an elevated level of understanding in the process of video and digital image processing. The proposed IoTDL – DRD method imparts the knowledge on the proposed subject matter to the computer vision, such that it can able to detect the diabetics retinopathy more effectively than the diagnosis through the conventional methodologies.

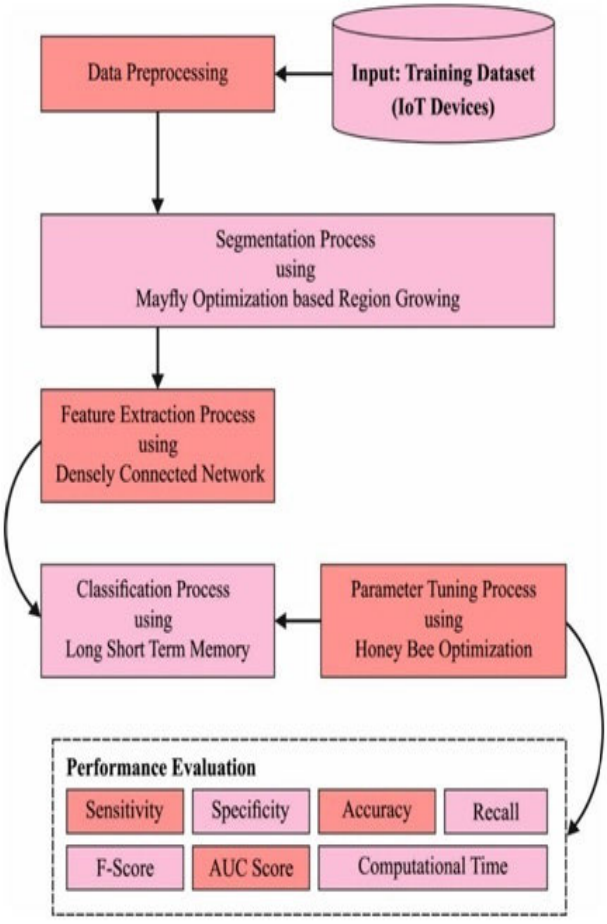

FIGURE 1. Block diagram of IoTDL-DRD approach.

B. IMAGE SEGMENTATION

Once the images are preprocessed, they are passed into the MRORG technique to segment the fundus images. Region growing (RG) is a pixel-based segmentation technique whereby the similarity constraint including intensity, texture, and so on, are taken into account for grouping the pixel into regions [19]. Initially, a collection of pixels is integrated with the help of iteration methodology. Next, the seed pixel is chosen alongside the regions and the group is supported by integrating with neighboring pixel that is corresponding and whereby it increases the region size.

The growth of region is ended whether the neighboring pixel doesn't satisfy the similarity constraint and another seed pixel is carefully chosen. Repeat the process until all the pixels in the image belongs to certain regions. In this work, seed point and threshold selection take a decision regarding the similarity condition because it plays a major part in enhancing the segmentation accuracy. As mammogram suffers from serious intensity variation, a constant threshold selection doesn't permit accurate segmentation. As a result, this work emphasizes increasing the automatic DA methodology for generating an optimal seed point and threshold. The step-wise procedure for region growing model is shown below.

a. Input the abnormal image.
b. Now, 't' characterizes the improved threshold generated using MFO approach
c. Place t as seed point for region growing model.
d. Add four adjacent pixels.
e. Estimate the distance (d) between the neighboring pixels and mean of region intensity.
f. Execute region growing if d $\leq$ t on four adjacent pixels and add all if they are't included before in the region and save the coordinate of the new pixel.
g. Store the mean of novel region and return to step 2 along with executing the region growing method until each pixel is gathered.

MFO is a new heuristic approach to solving complicated nonlinear optimization problems that were developed [20]. It was inclined by the reproduction process and behavior of MF. In time t, the MF position in a 2D search space is initialized by $a = (a_1, \ldots, a_d)^T$ and $b = (b_1, \ldots, b_d)^T$, correspondingly, and velocity $v = (v_1, \ldots, v_d)^T$ is allocated to every MF. The objective function (F) defines the performance of MF. In every iteration, the model saves the global positions (gbest) and best personal (pbest). One cycle (*Cyc*) is the period among the travel time for every visited node, sum of vacation charging, and two charging demands. The fitness function aim is to minimize system total power consumption, the number of cycles, and MC overall distance traveled that maximizes mobile charging vacation time.

$$\begin{aligned} F = &(\frac{Cyc}{10^{2\lfloor \log_{10} Cyc \rfloor}} - 1^{-8})^2 \\ &+(e_{\min} - 1^{-8})^2 + (e_{thresh} - 1^{-8})^2 \\ &+(\frac{1}{\tau_{vac}} - 1^{-8})^2 + (\frac{D_{total}}{10^{2\lfloor \log_{10} D_{total} \rfloor}} - 1^{-8})^2 \\ \text{s.t } &E_{\min} < e_{\min} < e_{thresh'} E_{\min} = 0.05 \times E_{\max} \\ &e_{\max} < e_{thresh} < E_{\max}, E_{\max} = 10.8\text{Kj} \end{aligned} \tag{1}$$

Every MF location is attuned based on own and neighbor proficiencies. The male MF velocity and position updating are shown below:

$$a_i^{t+1} = a_i^t + V_i^{t+1} \tag{2}$$

$$\begin{aligned} V_i^{t+1} = &g \times V_{ij}^t + x1 e^{-\beta_{n_p^2}} \left(pbest_{ij} - a_{ij}^t \right) \\ &+ x_2 e^{-\beta_{n_g^2}} \left(gbest_j - a_{ij}^t \right) \end{aligned} \tag{3}$$

Though it should remain in nuptial dance, the optimal male MF upgrades its velocity with the following expression

$$\mathrm{V_i^{t+1}} = \mathrm{V_i^t} + \mathrm{m} \times \mathrm{n} \tag{4}$$

$$b_i^{t+1} = b + V_i^{t+1} \tag{5}$$

The female MF location and velocity are upgraded in the following:

$$V_i^{t+1} = \begin{cases} g \times V_{ij}^t + x_{2^e}^{-\beta_{n_{mf}^2 (a_{ij}^t - b_{i)}^t}} & if\ f\ (b_i) > f(a_i) \\ g \times V_{ij}^t + fl \times n & if\ f\ (b_i) \leq f(a_i) \end{cases} \tag{6}$$

In Eq. (6), x_1 and x_2 indicates individual learning variable. g denotes the inertia weight, β refers to distance sight coefficient, m denotes the nuptial dance, and fl characterizes random flight, correspondingly. The Cartesian distance is signified as n_p and n_g, and n shows an arbitrary value between -1 and 1. Male MF is thought to move at a lower velocity in the nuptial dance, while female MF moves at a higher velocity in the arbitrary flight. Parent MF is selected to mate according to the fitness value. Accordingly, the higher the fitness values, the greater the probability of selection. The crossover operator portrays the mating of two MFs in the following: male and female population. Two off springs (children) are generated in the following:

$$M_{child1} = \ominus \times M_{male} + (1 - \ominus) \times M_{female} \tag{7}$$

$$M_{child2} = \ominus \times M_{female} + (1 - \ominus) \times M_{male} \tag{8}$$

M_{ale} signifies the male and M_{female} female parents $\ominus$ denote an arbitrary value within a provided range whereas the primary velocity of the children is fixed as zero. Afterward estimating the efficiency of the children, the mutation is presented. The model is avoided getting a local minimum by mutating the children. For inducing mutation in Eq. (8), a uniform distribution arbitrary value is included for chosen children.

$$M_{Child'\alpha} = M_{Child\alpha} + \sigma N_\alpha\ (0, 1) \tag{9}$$

In Eq. (9), σ and N_α denoted the standard deviation and uniform distributions, correspondingly. Also, the mutated children are assessed in terms of efficiency. The mutated children are combined with the non-mutated children, afterward, they are similarly distributed Parent and child population is arranged by efficiency to choose the following generation of MF for optimization.

C. FEATURE EXTRACTION

To derive optimal feature vectors, the DenseNet model is exploited in this study. The simple DenseNet is created by alternating transition and dense blocks followed by a Soft-Max classifier and fully connected layer [21]. The dense block is composed of two cascaded convolution layers comprised of batch normalization (BN), convolution, and leaky rectified linear unit (LReLU) layers "BN-Conv-LReL"). Initially, the dense block makes use of 1 × 1 kernel size for producing 4r output feature map whereas the next generate r feature map with 3 × 3 kernel size, where r is a pre-determined constant and set as 32. The dense blocks concatenate r output feature map with the input map, thus resulting in increased number of maps. The transition block comprises average pooling and convolution layers with 2 × 2 pool sizes. Here, the output feature map count in the transition block is similar to input. In this work,"conv" implies a convolution uni;"1 × 1 × 64 conv" denotes the convolution layer in the unit that makes use of the 1 × 1 kernel size for producing 64 output feature map;"2 × 2 pool" represents an average pooling layer with 2 × 2 pool siz;θ represents the number of concluding output classe;"[·] × " indicates the structure"[·]" is cascaded repeatedly for more than one times. There exists one FC layer and twenty three convolution layer that is much shallower than that of the original DenseNet with 121 convolution layers.

D. IMAGE CLASSIFICATION

For DR recognition and classification, the HBO algorithm with LSTM model is exploited in this study. The most

important algorithm of DL methods is CNN. In the study, the hybrid amalgamation of LSTM together with CNN is exploited [22]. Honey bees exhibit a variety of complex behaviors in nature, including mating, reproduction, and foraging. Several honey bee-based optimization algorithms have imitated these behaviors. Honey Bees Optimization is a well-known algorithm that was inspired by the mating and breeding behavior of honeybees (HBO). The algorithm begins with a single queen that has no family and progresses to the growth of a colony that has families that contain one or more queens. A colony of honey bees can access numerous food sources in expansive fields and can fly up to 11 km to do so. About one-fourth of the colony's bees work as foragers. Scout bees start the foraging process by looking for promising flower patches. During the harvesting season, a portion of the scout bees are kept by the colony. The scout bees will search farther after discovering a flower patch in the hopes of discovering one that is even better. Randomly, the scout bees look for the best patches. An artificial neural network called Long Short-Term Memory (LSTM) is employed in deep learning and artificial intelligence. LSTM has feedback connections as opposed to typical feedforward neural networks. Such a recurrent neural network (RNN) can process entire data sequences in addition to single data points (such as images). In order to process the consecutive dataset, RNN is broadly employed. The existing input and the previous output are connected to each other through these RNN models. The tanh activation functionthereby controls it, such that the series state has been taken into account. In time t, the derivative RNN would communicate and spread to time $t-1, t-2, \ldots, l$, thus resulting in the presence of a multiplicative factor. Gradient disappearance and explosion occur if there exists endless multiplication. In the forward procedure, the input of starting series has negligible or small effects on the later happening sequence, and consequently, it is regarded as a key challenge of loss distance dependency. By familiarizing numerous gating models, LSTM could resolve the problem easily. For a sigmoid operation, the contemporary input in a function X_t and the previous output h_{t-1} are provided as an input such that values among zero and one are produced, thus defining the existing novel data that could be effortlessly maintained. The comprehensive state C_t of the following moment is attained using input and forget gates, and it is employed for the initiation of the hidden state h_t of the subsequent layer, thus establishing the output of the existing units. The description of the output can be performed through the output gate regarding the data attained from the cell state. A sigmoid function similar to input gate that produces a value 0_t among zero and one, which illustrates the quantity of cell state data described for projecting them as output. Figure 2 illustrates the design of a standard LSTM layer using appropriate inputs and outputs. For the LSTM, the respective alliances among the different gates are arithmetically formulated in the subsequent expression:

$$z_t = \tanh(W_z[h_{t-1}, X_t] + b_z)$$
$$i_t = sigmoid(W_i[h_{t-1}, X_t] + b_i)$$
$$f_t = sigmoid\left(W_f\,[h_{t-1}, X_t] + b_f\right)$$
$$o_t = sigmoid(W_o[h_{t-1}, X_t] + b_o)$$
$$c_t = f_t \cdot C_{t-1} + i_t \cdot z_t$$
$$h_t = 0_t \cdot \tanh(c_t) \tag{10}$$

At the end stage, the HBO algorithm is exploited for optimal hyper parameter adjustment process. A honeybee (HB) colony could fly up to 11 km for exploiting food sources and might attempt to terminate larger areas with large sources of food [23]. The cycle of forager starts with the hunt by scout bee for enticing flower patch. Once the scout bee discovers the flower patch, they should search in advance to determine the best patch. The scout bee is desperately searching to discover the optimal spots.

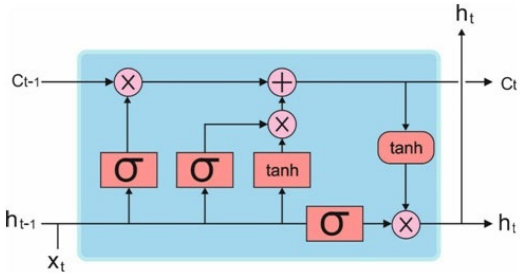

FIGURE 2. Structure of LSTM.

During the hive, the scout bee acts as the counterpart regarding the nature of food sources, on the basis of the sugar content, amongst others. The scout bee injects its nectar and later goes ahead of the hive for celebrating the ballet, termed waggle dance, with others. The waggle dance is modeled afterward the wagging run (the performer makes a loud buzzing rhythm and moves the body simultaneously) that the scout be used to transmit the residual parts of the community data on the food sources. The scout bee offers this data via waggle dance; consistency and distance from the path and hive sources. The waggle direction has eight-shaped patterns. First, the scout bees make a noise using their wing muscles which produces a loud buzz, and start to run in a vertical direction in a straight line which indicates the path for sun azimuth at the square and food source location. Instead, scouts circle back and transform left and right.

The HBO algorithm derives a Fitness Function (FF) for obtaining enhanced performance of the classification. It sets an optimistic numeral to characterize the good outcome of the candidate solution. The minimization of the classifier error rate has been taken as the FF in this study, as demonstrated in Eq. (11). The worse solution accomplishes the highest error rate and the optimum solution has the lowest error rate.

$$\begin{aligned} fitness\,(x_i) &= Classifier\ Error\ Rate\ \ (x_i) \\ &= \frac{number\ of\ misclassified\ samples}{Total\ number\ of\ samples} * 100 \end{aligned} \tag{11}$$

TABLE 1. Pseudocode of HBO algorithm.

ALGORITHM 1: Pseudocode of HBO Algorithm

- Instantiation of the parameter value of size of population (N), ps for optimum patch size, ep for elite patch size, fr for the amount of forager bees employed to the elite site, np signifies the amount of forager bees nearby the non-elite optimum patch, nb shows the neighborhood size, Mox characterizes maximal amount of iteration, err denotes error limits.
- Express the fitness function.
- Order the initialized population based on fitness outcome
- While $k \leq$ Max or $Fitnessvalue_k - Fitnessvalue_{k-1} \leq err$
- $K = k + 1$
- For neighborhood search chooses the Elite patch includes the optimal non-elite patch.
- Train the foraging bee to the elite patch with non-elite optimal patch.
- Inspect every patch of fitness values.
- Group the outcome based on the fitness.
- Allocate the residual bees for non-optimum location of global search.
- Determine the non-optimum patch fitness values.
- Arrange the cumulative outcomes based on fitness.
- Repeat the process until the ending condition is met.
- Stop

IV. RESULTS AND DISCUSSION

The performance validation of the IoTDL-DRD method is validated utilizing MESSIDOR dataset [24]. It comprises 1744 fundus images under five class labels as shown in Table 2. The presented IoTDL-DRD method can be simulated utilizing Python tool. Some sample images are depicted in Figure 3. Figure 4 illustrates the confusion matrices derived by the IoTDL-DRD model on varying training (TR) and testing (TS) data. With 80% of TR data, the IoTDL-DRD method has classified 813 samples into normal, 203 samples into mild, 267 samples into moderate, 52 samples into severe,

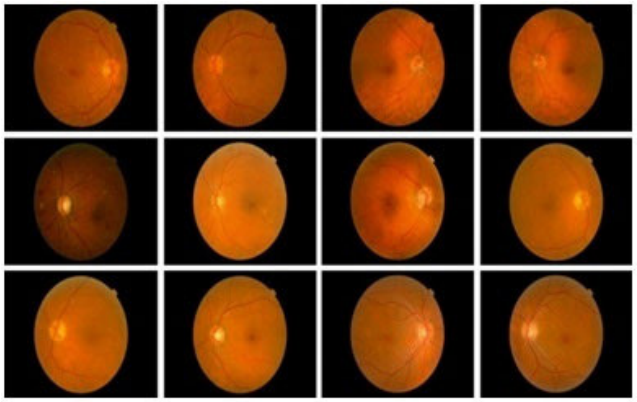

FIGURE 3. Sample images.

TABLE 2. Dataset details.

Class	Number of Samples
Normal	1017
Mild	270
Moderate	347
Severe	75
PDR	35
Total Number of Samples	1744

and 24 samples into PDR. In addition, with 20% of TS data, IoTDL-DRD method has classified 181 samples into normal, 60 samples into mild, 77 samples into moderate, 17 samples into severe, and 6 samples into PDR. Finally, with 70% of TR data, the IoTDL-DRD approach has classified 699 samples into normal, 175 samples into mild, 224 samples into moderate, 31 samples into severe, and 1 sample into PDR. Finally, with 30% of TS data, the IoTDL-DRD method has classified 296 samples into normal, 78 samples into mild, 93 samples into moderate, 13 samples into severe, and 3 samples into PDR.

The fundus images used in the proposed work possess sharp margins with normal RGB pattern. The fundus images have normal features including the optic disc, fovea and blood vessels. The images have smaller central cup with a normal background. Table 3 exhibits the DR classification outcomes of the IoTDL-DRD model on 80% of TR data and 20% of TS data. These table values demonstrate the improved performance of the IoTDL-DRD model. The dataset is fed with the normal sample of 1017, 270 samples with mild diabetics, 347 samples with moderate illness, 75 samples with severe while 35 samples with PDR level. The Figure 4 depicts the confusion matrix of IoTDL – DRD approach with 80% of TR data, 20% of TS data, 70% of TR data and 30% of TS data respectively. From this confusion matrix, 58.28% were found to be normal, 14.55% were reported with mild diabetics, 19.14% as a moderate level of diabetics and 3.73% with a severe level of diabetics retinopathy having more chances of loss of eyesight. The IoT captured images were stored in the database and is employed for the analysis purposes.

Figure 5 offers a brief set of DR classification performance of the IoTDL-DRD model on 80% of TR data. The method has classified fundus image into normal class with $accu_y$, $sens_y$, $spec_y$, F_{score}, AUC_{score}, and MCC of 98.14%, 97.72%, 98.76%, 98.43%, 98.24%, and 96.16% respectively. The high level of performance in the aforementioned parameters is possibly achieved by incorporating the Deep learning models in the diagnosis of DR.

Similarly, the IoTDL-DRD technique has categorized fundus image into mild class with $accu_y$, $sens_y$, $spec_y$, F_{score}, AUC_{score}, and MCC of 98.78%, 97.13%, 99.07%, 95.98%, 98.10%, and 95.27% correspondingly. It has categorized fundus image into moderate class with $accu_y$, $sens_y$,

TABLE 3. Result analysis of IoTDL-DRD approach with distinct class labels under 70:30 of TR/TS data.

Labels	Accuracy	Sensitivity	Specificity	F-Score	AUC Score	MCC
Training Phase (80%)						
Normal	98.14	97.72	98.76	98.43	98.24	96.16
Mild	98.78	97.13	99.07	95.98	98.10	95.27
Moderate	98.92	98.89	98.93	97.27	98.91	96.62
Severe	99.28	92.86	99.55	91.23	96.20	90.87
PDR	99.71	85.71	100.00	92.31	92.86	92.45
Average	**98.97**	**94.46**	**99.26**	**95.04**	**96.86**	**94.27**
Testing Phase (20%)						
Normal	98.28	97.84	98.78	98.37	98.31	96.56
Mild	99.14	98.36	99.31	97.56	98.83	97.04
Moderate	99.14	100.00	98.90	98.09	99.45	97.56
Severe	99.43	89.47	100.00	94.44	94.74	94.31
PDR	99.43	85.71	99.71	85.71	92.71	85.42
Average	**99.08**	**94.28**	**99.34**	**94.84**	**96.81**	**94.18**

TABLE 4. Result analysis of IoTDL-DRD approach with distinct class labels under 70:30 of TR/TS data.

Labels	Accuracy	Sensitivity	Specificity	F-Score	AUC Score	MCC
Training Phase (70%)						
Normal	96.23	97.90	93.87	96.81	95.89	92.23
Mild	97.46	93.58	98.16	91.86	95.87	90.38
Moderate	95.41	91.06	96.51	88.89	93.78	86.04
Severe	97.79	58.49	99.57	69.66	79.03	69.94
PDR	98.36	05.00	99.92	09.09	52.46	15.43
Average	**97.05**	**69.21**	**97.61**	**71.26**	**83.41**	**70.80**
Testing Phase (30%)						
Normal	95.42	97.69	92.31	96.10	95.00	90.62
Mild	98.28	93.98	99.09	94.55	96.53	93.53
Moderate	96.18	92.08	97.16	90.29	94.62	87.94
Severe	96.76	59.09	98.41	60.47	78.75	58.79
PDR	97.71	20.00	100.00	33.33	60.00	44.20
Average	**96.87**	**72.57**	**97.39**	**74.95**	**84.98**	**75.02**

$spec_y$, F_{score}, AUC_{score}, and MCC of 98.92%, 98.89%, 98.93%, 97.27%, 98.91%, and 96.62% correspondingly. Finally, it has categorized fundus image into severe classes with $accu_y$, $sens_y$, $spec_y$, F_{score}, AUC_{score}, and MCC of 99.28%, 92.86%, 99.55%, 91.23%, 96.20%, and 90.87% correspondingly.

Figure 6 provides a detailed set of DR classification performance of the IoTDL-DRD method on 20% of TS data. The IoTDL-DRD algorithm has categorized fundus image into normal class with $accu_y$, $sens_y$, $spec_y$, F_{score}, AUC_{score}, and MCC of 98.28%, 97.84%, 98.78%, 98.37%, 98.31%, and 96.56% correspondingly. Also, it has categorized fundus image into mild class with $accu_y$, $sens_y$, $spec_y$, F_{score}, AUC_{score}, and MCC of 99.14%, 98.36%, 99.31%, 97.56%, 98.83%, and 97.04% correspondingly. It has categorized fundus image into moderate class with $accu_y$, $sens_y$, $spec_y$, F_{score}, AUC_{score}, and MCC of 99.14%, 100%, 98.90%, 98.09%, 99.45%, and 97.56% correspondingly. Finally, it has categorized fundus image into severe classes with $accu_y$, $sens_y$, $spec_y$, F_{score}, AUC_{score}, and MCC of 99.43%, 89.47%, 100%, 94.44%, 94.74%, and 94.31% correspondingly.

Table 4 exhibits the DR classification outcomes of the IoTDL-DRD model on 70% of TR data and 30% of TS data.

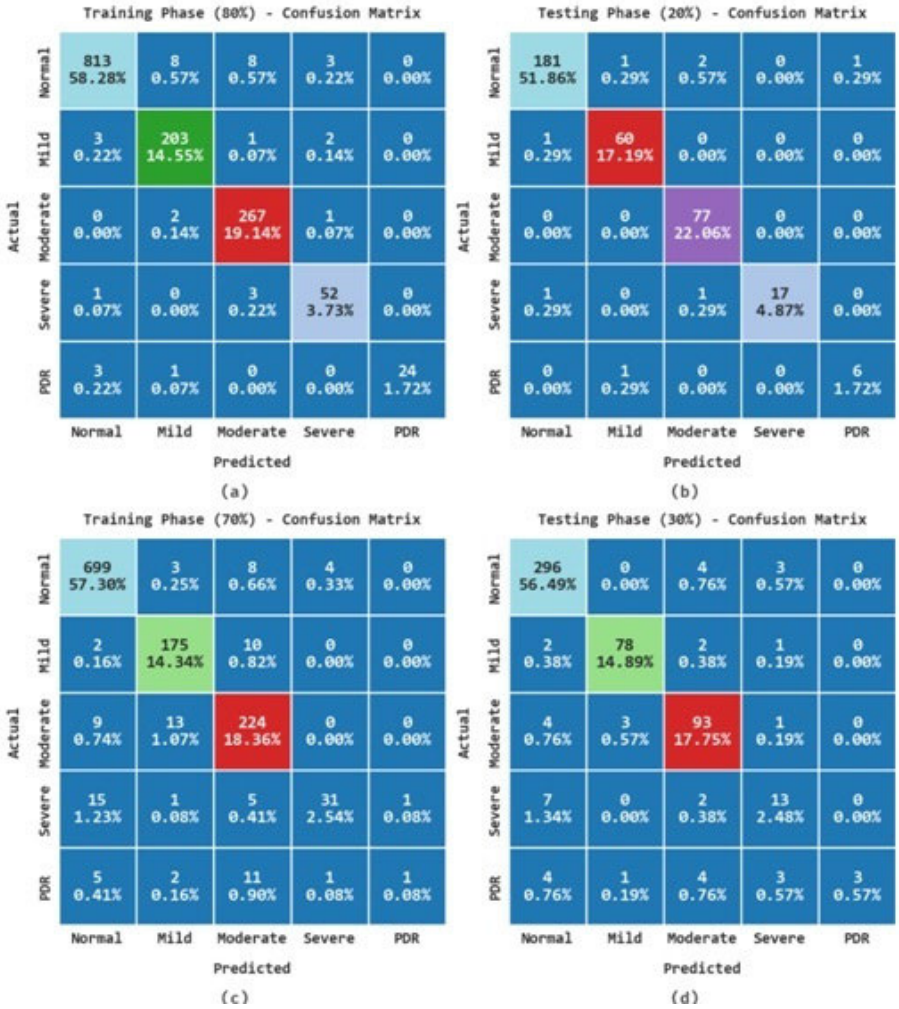

FIGURE 4. Confusion matrices of IoTDL-DRD approach (a) 80% of TR data, (b) 20% of TS data, (c) 70% of TR data, and (d) 30% of TS data.

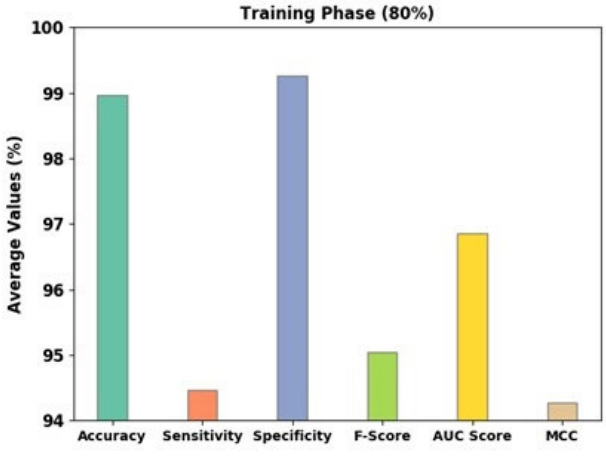

FIGURE 5. Average analysis of IoTDL-DRD approach under 80% of TR data.

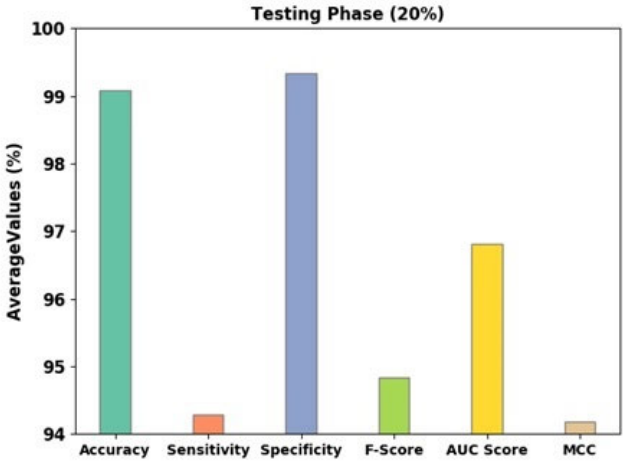

FIGURE 6. Average analysis of IoTDL-DRD approach under 20% of TS data.

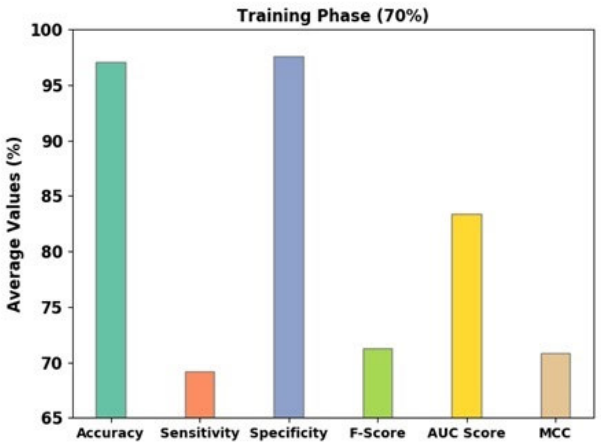

FIGURE 7. Average analysis of IoTDL-DRD approach under 70% of TR data.

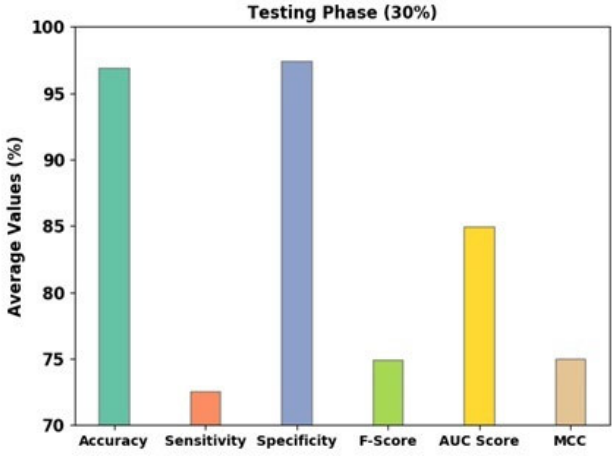

FIGURE 8. Average analysis of IoTDL-DRD approach under 30% of TS data.

FIGURE 9. TRA and VLA analysis of IoTDL-DRD approach.

These table values demonstrate the improved performance of the IoTDL-DRD model.

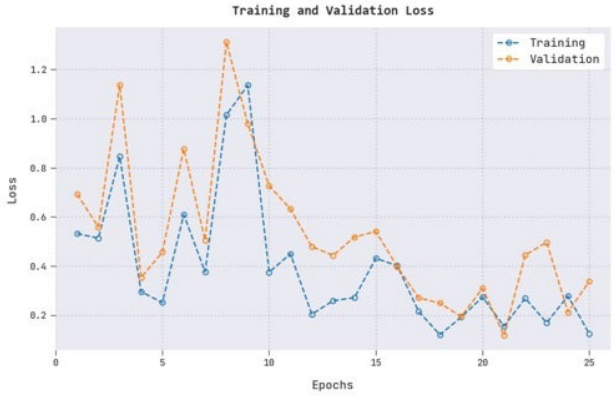

FIGURE 10. TRL and VLL analysis of IoTDL-DRD approach.

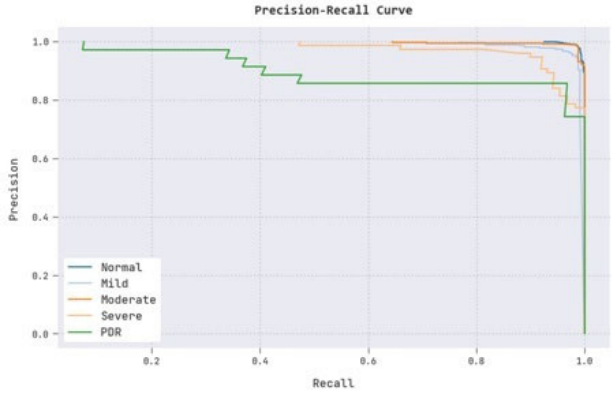

FIGURE 11. Precision-recall analysis of IoTDL-DRD approach.

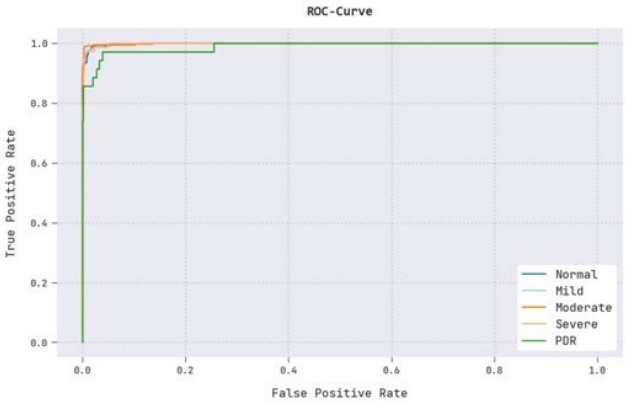

FIGURE 12. ROC analysis of IoTDL-DRD approach.

Figure 7 presents a complete set of DR classification performances of the IoTDL-DRD approach on 70% of TR data. The IoTDL-DRD algorithm has classified fundus image into normal class with $accu_y$, $sens_y$, $spec_y$, F_{score}, AUC_{score}, and MCC of 96.23%, 97.90%, 93.87%, 96.81%, 95.89%, and 92.23% correspondingly.

Similarly, it has categorized fundus image into mild class with $accu_y$, $sens_y$, $spec_y$, F_{score}, AUC_{score}, and MCC of

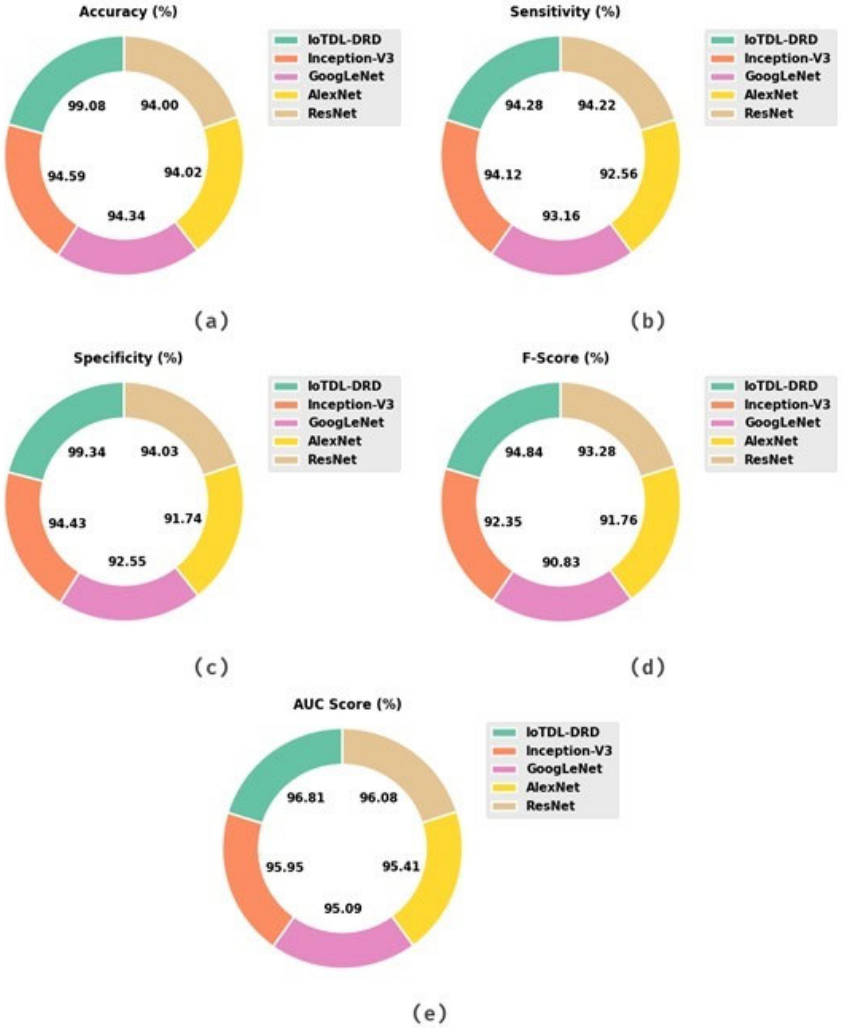

FIGURE 13. Comparatives analysis of IoTDL-DRD approach (a) $Accu_y$, (b) $Sens_y$, (c) $Spec_y$, (d) F_{score}, and (e) AUC_{score}.

97.46%, 93.58%, 98.16%, 91.86%, 95.87%, and 90.38% correspondingly. Simultaneously, it has categorized fundus image into moderate class with $accu_y$, $sens_y$, $spec_y$, F_{score}, AUC_{score}, and MCC of 95.41%, 91.06%, 96.51%, 88.89%, 93.78%, and 86.04% correspondingly. Meanwhile, the IoTDL-DRD approach has categorized fundus image into severe classes with $accu_y$, $sens_y$, $spec_y$, F_{score}, AUC_{score}, and MCC of 97.79%, 58.49%, 99.57%, 69.66%, 79.03%, and 69.94% correspondingly.

Figure 8 demonstrates a detailed set of DR classification performance of the IoTDL-DRD approach on 30% of TS data. The method has categorized fundus image into normal class with $accu_y$, $sens_y$, $spec_y$, F_{score}, AUC_{score}, and MCC of 95.42%, 97.69%, 92.31%, 96.10%, 95%, and 90.62% correspondingly. Also, it has categorized fundus image into mild class with $accu_y$, $sens_y$, $spec_y$, F_{score}, AUC_{score}, and MCC of 98.28%, 93.98%, 99.09%, 94.55%, 96.53%, and 93.53% correspondingly. In the meantime, it has categorized fundus image into moderate class with $accu_y$, $sens_y$, $spec_y$, F_{score}, AUC_{score}, and MCC of 96.18%, 92.08%, 97.16%, 90.29%, 94.62%, and 87.94% individually. Eventually, it has categorized fundus image into severe class with $accu_y$, $sens_y$, $spec_y$, F_{score}, AUC_{score}, and MCC of 96.76%, 59.09%, 98.41%, 60.47%, 78.75%, and 58.79% correspondingly.

The training accuracy (TRA) and validation accuracy (VLA) gained by IOTDL-DRD methodology on test dataset is shown in Figure 9. The experimental outcome denoted the IOTDL-DRD approach has exhibited maximal values of TRA and VLA. Seemingly the VLA is greater than TRA. The training loss (TRL) and validation loss (VLL) attained by the IOTDL-DRD methodology on test dataset are exhibited in Figure 10. The experimental result represented the IOTDL-DRD approach has shown least values of TRL and VLL. Particularly, the VLL is lesser than TRL. An obvious precision-recall analysis of the IOTDL-DRD system on test dataset is shown in Figure 11. The figure stated that the

TABLE 5. Result analysis of IoTDL-DRD approach with distinct class labels under 70:30 of TR/TS data.

Labels	Accuracy	Sensitivity	Specificity	AUC Score	MCC	Computational Time
IoTDL-DRD	99.08	94.28	99.34	94.84	96.81	11.21 ms
Inception-V3	94.59	94.12	94.43	92.35	95.95	18.56 ms
GoogLeNet	94.34	93.16	92.55	90.83	95.09	21.69 ms
AlexNet	94.02	92.56	91.74	91.76	95.41	29.48 ms
ResNet	94.00	94.22	94.03	93.28	96.08	35.65 ms

IOTDL-DRD technique has resulted in higher values of precision-recall values in all classes. A brief ROC study of the IOTDL-DRD method on test dataset was depicted in Figure 12. The outcomes represented by the IOTDL-DRD method has revealed its capability in categorizing distinct classes on test dataset.

For assuring the enhanced DR classification performance of the IoTDL-DRD model, a wide ranging comparative analysis is made in Table 5 and Figure 13 [25]. The fallouts highlighted the IoTDL-DRD model has shown enhanced outcomes over other models [26]. Based on $accu_y$, the IoTDL-DRD model has offered higher $accu_y$ of 99.08% whereas the Inception-v3, GoogLeNet, AlexNet, and ResNet models have attained lower $accu_y$ of 94.59%, 94.34%, 94.02%, and 94% respectively. Similarly, according to $sens_y$, the IoTDL-DRD approach has obtainable superior $sens_y$ of 94.28% whereas the Inception-v3, GoogLeNet, AlexNet, and ResNet techniques have attained lower $sens_y$ of 94.12%, 93.16%, 92.56%, and 94.22% correspondingly.

Likewise, based on F_{score}, the IoTDL-DRD technique has existing superior F_{score} of 94.84% whereas the Inception-v3, GoogLeNet, AlexNet, and ResNet systems have reached lesser F_{score} of 92.35%, 90.83%, 91.76%, and 93.28% correspondingly. Therefore, the experimental results [27] verified that the IoTDL-DRD model has accomplished enhanced DR classification performance over other DL models [28]. The computational time for the proposed process is computed and is observed to possess a reduced duration of 11.21 msec. This observed value is proved to be lesser than the other computer vision processes [29].

V. CONCLUSION

In this paper, a novel IoTDL-DRD model was developed for DR detection and classification on retinal fundus images. The presented IoTDL-DRD method allows the IoT devices for data collection purposes and then transfers to the cloud server to process them. Then, the retinal fundus images are preprocessed for noise removal and contrast improvement. Afterward, the MFORG technique can be employed for lesion segmentation in the fundus images. For DR recognition and classification, the HBO algorithm with LSTM model is exploited in this study. For evaluating the improved DR diagnostic outcomes of the IoTDL-DRD technique, a comprehensive set of simulations were carried out. A wide ranging comparison study reported the superior performance of the presented model compared to recent state of art approaches. In upcoming years, deep instance segmentation models were derived to boost the classification results.

ACKNOWLEDGMENT

The authors extend their appreciation to ''the Deputyship for Research & Innovation, Ministry of Education in Saudi Arabia for funding this research work through the project number G: 693-144-1443'' and King Abdulaziz University, Deanship of Scientific Research (DSR), Jeddah, Saudi Arabia.

REFERENCES

[1] D. S. W. Ting, H. Lin, P. Ruamviboonsuk, T. Y. Wong, and D. A. Sim, ''Artificial intelligence, the Internet of Things, and virtual clinics: Ophthalmology at the digital translation forefront,'' *Lancet Digit. Health*, vol. 2, no. 1, pp. e8–e9, Jan. 2020.

[2] K. Parthiban and K. Venkatachalapathy, ''Internet of Things and cloud enabled hybrid feature extraction with adaptive neuro fuzzy inference system for diabetic retinopathy diagnosis,'' *J. Comput. Theor. Nanosci.*, vol. 17, no. 12, pp. 5261–5269, Dec. 2020.

[3] J. T. Kelly, K. L. Campbell, E. Gong, and P. Scuffham, ''The Internet of Things: Impact and implications for health care delivery,'' *J. Med. Internet Res.*, vol. 22, no. 11, Nov. 2020, Art. no. e20135.

[4] R. J. Kavitha, T. Avudaiyappan, T. Jayasankar, and J. Selvi, ''Industrial Internet of Things (IIoT) with cloud teleophthalmology-based age-related macular degeneration (AMD) disease prediction model,'' in *Smart Sensors for Industrial Internet of Things*. Cham, Switzerland: Springer, 2021, pp. 161–172.

[5] A. B. Tufail, I. Ullah, W. U. Khan, M. Asif, I. Ahmad, Y.-K. Ma, R. Khan, and M. S. Ali, ''Diagnosis of diabetic retinopathy through retinal fundus images and 3D convolutional neural networks with limited number of samples,'' *Wireless Commun. Mobile Comput.*, vol. 2021, pp. 1–15, Nov. 2021.

[6] T. J. Jebaseeli, J. David, and V. Jegathesan, ''Machine learning and Internet of Things techniques to assist the type I diabetic patients to predict the regular optimal insulin dosage,'' in *Internet of Medical Things*. Cham, Switzerland: Springer, 2021, pp. 159–174.

[7] V. Ramalingam, D. B. Mariappan, R. Gopal, and K. M. Baalamurugan, ''An effective social Internet of Things (SIoT) model for malicious node detection in wireless sensor networks,'' in *Artificial Intelligence Techniques in IoT Sensor Networks*. Boca Raton, FL, USA: CRC Press, 2020, pp. 181–195.

[8] E. A. Refaee and S. Shamsudheen, ''A computing system that integrates deep learning and the Internet of Things for effective disease diagnosis in smart health care systems,'' *J. Supercomput.*, vol. 78, no. 7, pp. 9285–9306, May 2022.

[9] S. M. Zobaed, M. Hassan, M. U. Islam, and M. E. Haque, ''Deep learning in IoT-based healthcare applications,'' in *Deep Learning for Internet of Things Infrastructure*. Boca Raton, FL, USA: CRC Press, 2021, pp. 183–200.

[10] X. Ma, T. Yao, M. Hu, Y. Dong, W. Liu, F. Wang, and J. Liu, "A survey on deep learning empowered IoT applications," *IEEE Access*, vol. 7, pp. 181721–181732, 2019.
[11] R. Rajavel, B. Sundaramoorthy, K. Gr, S. K. Ravichandran, and K. Leelasankar, "Cloud-enabled diabetic retinopathy prediction system using optimized deep belief network classifier," *J. Ambient Intell. Humanized Comput.*, vol. 2022, pp. 1–9, Jul. 2022.
[12] A. M. Dayana and W. R. Emmanuel, "Deep learning enabled optimized feature selection and classification for grading diabetic retinopathy severity in the fundus image," *Neural Comput. Appl.*, vol. 34, pp. 1–21, Jun. 2022.
[13] J. G. R. Elwin, J. Mandala, B. Maram, and R. R. Kumar, "Ar-HGSO: Autoregressive-Henry gas sailfish optimization enabled deep learning model for diabetic retinopathy detection and severity level classification," *Biomed. Signal Process. Control*, vol. 77, Aug. 2022, Art. no. 103712.
[14] N. O. Aljehane, "An intelligent moth flame optimization with inception network for diabetic retinopathy detection and grading," in *Proc. 2nd Int. Conf. Comput. Inf. Technol. (ICCIT)*, Jan. 2022, pp. 370–373.
[15] K. Gunasekaran, R. Pitchai, G. K. Chaitanya, D. Selvaraj, S. A. Sheryl, H. S. Almoallim, S. A. Alharbi, S. S. Raghavan, and B. G. Tesemma, "A deep learning framework for earlier prediction of diabetic retinopathy from fundus photographs," *BioMed Res. Int.*, vol. 2022, pp. 1–15, Jun. 2022.
[16] I. K. Gupta, A. Choubey, and S. Choubey, "Mayfly optimization with deep learning enabled retinal fundus image classification model," *Comput. Electr. Eng.*, vol. 102, Sep. 2022, Art. no. 108176.
[17] J. Latif, S. Tu, C. Xiao, S. U. Rehman, A. Imran, and Y. Latif, "ODGNet: A deep learning model for automated optic disc localization and glaucoma classification using fundus images," *Social Netw. Appl. Sci.*, vol. 4, no. 4, pp. 1–11, Apr. 2022.
[18] N. Al-Saiyd and S. Talafha, "Mammographic image enhancement tachniques—A survey," *Int. J. Comput. Sci. Inf. Technol. Secur.*, vol. 5, pp. 200–206, Jan. 2015.
[19] M. A. Mohammed, M. K. Abd Ghani, R. I. Hamed, D. A. Ibrahim, and M. K. Abdullah, "Artificial neural networks for automatic segmentation and identification of nasopharyngeal carcinoma," *J. Comput. Sci.*, vol. 21, pp. 263–274, Jul. 2017.
[20] M. A. M. Shaheen, H. M. Hasanien, M. S. E. Moursi, and A. A. El-Fergany, "Precise modeling of PEM fuel cell using improved chaotic MayFly optimization algorithm," *Int. J. Energy Res.*, vol. 45, no. 13, pp. 18754–18769, Oct. 2021.
[21] Z. Huang, X. Zhu, M. Ding, and X. Zhang, "Medical image classification using a light-weighted hybrid neural network based on PCANet and DenseNet," *IEEE Access*, vol. 8, pp. 24697–24712, 2020.
[22] J. Lei, C. Liu, and D. Jiang, "Fault diagnosis of wind turbine based on long short-term memory networks," *Renew. Energy*, vol. 133, pp. 422–432, Apr. 2019.
[23] S. Nayak, C. Kumar, S. Tripathi, N. Mohanty, and V. Baral, "Regression test optimization and prioritization using honey bee optimization algorithm with fuzzy rule base," *Soft Comput.*, vol. 25, no. 15, pp. 9925–9942, Aug. 2021.
[24] X. Zhang, G. Cazuguel, B. Lay, B. Cochener, C. Trone, and P. Gain, "Feedback on a publicly distributed image database: The Messidor database," *Image Anal. Stereol.*, vol. 33, pp. 231–234, Aug. 2014.
[25] A. Bilal, L. Zhu, A. Deng, H. Lu, and N. Wu, "AI-based automatic detection and classification of diabetic retinopathy using U-Net and deep learning," *Symmetry*, vol. 14, no. 7, p. 1427, Jul. 2022.
[26] O. M. Al-Hazaimeh, A. Abu-Ein, N. Tahat, M. Al-Smadi, and M. Al-Nawashi, "Combining artificial intelligence and image processing for diagnosing diabetic retinopathy in retinal fundus images," *Int. J. Online Biomed. Eng.*, vol. 18, no. 13, pp. 131–151, Oct. 2022.
[27] N. Gharaibeh, O. M. Al-Hazaimeh, B. Al-Naami, and K. M. Nahar, "An effective image processing method for detection of diabetic retinopathy diseases from retinal fundus images," *Int. J. Signal Imag. Syst. Eng.*, vol. 11, pp. 206–216, Jan. 2018.
[28] N. Gharaibeh, O. M. Al-hazaimeh, A. Abu-Ein, and K. M. Nahar, "A hybrid SVM Naïve-Bayes classifier for bright lesions recognition in eye fundus images," *Int. J. Electr. Eng. Informat.*, vol. 13, no. 3, pp. 530–545, Sep. 2021.
[29] V. Conti, C. Militello, L. Rundo, and S. Vitabile, "A novel bio-inspired approach for high-performance management in service-oriented networks," *IEEE Trans. Emerg. Topics Comput.*, vol. 9, no. 4, pp. 1709–1722, Oct. 2021.

THANGAM PALANISWAMY (Member, IEEE) received the B.E. degree in computer hardware and software engineering from Avinashilingam University, India, in 2001, and the M.E. degree in computer science and engineering and the Ph.D. degree in information and communication engineering from Anna University, India, in 2007 and 2013, respectively. She has a total teaching experience of 15 years in various reputed engineering colleges in Tamil Nadu. She is currently an Associate Professor with the Department of Electrical and Computer Engineering, King Abdulaziz University, Saudi Arabia. Her research interests include databases, data processing and mining, medical image analysis, image processing, cryptography, embedded systems, and the Internet of Things. Her contributions in professional societies include IEEE, International Association of Engineers, Indian Society for Technical Education, and International Association of Computer Science and Information Technology.

MAHENDIRAN VELLINGIRI received the B.E. degree in electrical and electronics engineering from Maharaja Engineering College, Avinasi, affiliated to Bharathiyar University, Coimbatore, Tamil Nadu, in 2000, the M.E. degree in power electronics and drives from K. S. Rangasamy College of Technology, Tiruchengode, affiliated to Anna University, Chennai, Tamil Nadu, in 2006, and the Ph.D. degree in electrical engineering from Anna University, India, in 2014. He is currently an Assistant Professor with the Department of Electrical and Computer Engineering, King Abdulaziz University, Jeddah, Saudi Arabia. His research interests include soft computing applications in the control of power electronics drives, control systems, electrical machines, solar energy, and power systems.